THE JOURNAL OF PHYSICAL CHEMISTRY Letters

Letter

Cite This: J. Phys. Chem. Lett. 2018, 9, 5630−5635

pubs.acs.org/JPCL

Revealing the Activity Distribution of a Single Nanocatalyst by Locating Single Nanobubbles with Super-Resolution Microscopy

Ting Zhang,[†,‡] Shuping Li,[‡] Ying Du,[‡] Ting He,[‡] Yangbin Shen,[‡] Chuang Bai,[‡] Yunjie Huang,*[,†] and Xiaochun Zhou*[,‡,§]

[†]Faculty of Materials Science and Chemistry, China University of Geosciences, Wuhan 430074, China

[‡]Division of Advanced Nanomaterials, Suzhou Institute of Nano-tech and Nano-bionics, Chinese Academy of Sciences (CAS), Suzhou 215123, China

[§]Key Lab of Nanodevices and Applications, Suzhou Institute of Nano-Tech and Nano-Bionics, Chinese Academy of Sciences (CAS), Suzhou 215123, China

Supporting Information

ABSTRACT: It is challenging to uncover the catalytic activity at different locations of a single nanocatalyst for gas-generating reactions in real time. This research uses super-resolution microscopy to localize the center of single nanobubbles and reveal the local activity distribution at several to tens of nanometers accuracy. The distances between the centers of the nanobubbles and the center of the nanoplate usually distribute in a certain range from 0 to 500 nm, with the maximum population exhibiting at ∼200 nm. This research also shows that more nanobubbles appear near the tips of the Pd−Ag nanoplate compared with the edges, which indicates higher activity at the tips. In addition, the relationship between the location, lifetime, and turnover rate of the nanobubbles was also carefully studied. This work presents an effective, high-resolution method to localize the activity distribution of nanocatalysts during gas-generating reactions, such as photocatalytic water splitting, dehydrogenation, and electro-oxidation.

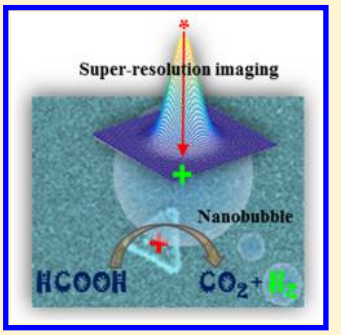

The catalytic activity at different locations of a nanocatalyst can vary greatly due to the different facets,[1] defects,[2−4] ligand/surfactant coverage,[5,6] composition,[7,8] structure,[9] and so on at these locations. Many methods, such as scanning tunneling microscopy (STM),[10,11] scanning electrochemical microscopy (SECM),[12,13] and optical super-resolution microscopy (SRM)[14−16] have been developed to detect the local activity with resolutions from subnanometer to several tens of nanometers. Of these, SRM uses visible light to detect the emission center of microscopic objects, such as a single molecule,[17,18] a nanoparticle,[19,20] or a small "hot spot".[21−23] Therefore, SRM has many advantages, including high time resolution (ms), atmospheric pressure, near room temperature, and nondestructive detection.

It is widely acknowledged that gas-generating catalysis is important to many energy-related research fields, such as photocatalytic water splitting,[24−27] water electrolysis,[28] dehydrogenation,[29−35] and the electro-oxidation of small organic molecules, including methanol,[36] ethanol,[37] and formic acid (FA).[38] Therefore, research on the local activity of nanocatalysts for gas-generating catalysis is in high demand. Researchers are now finding nanobubbles to be an effective way to study the activity and stability of these catalytic reactions at the single-nanoparticle level.[39−43] This is because surface nanobubbles have some unique properties: They have good stability and can last longer than expected against violent decompression.[16,44]

Usually, nanobubbles are investigated by atomic force microscopy (AFM),[45−47] electrochemical techniques,[42,43,48] total internal reflection fluorescence microscopy (TIRFM),[49] infrared spectroscopy,[50] and dark-field microscopy (DFM).[51,52] DFM is an especially effective method for monitoring the evolution of single nanobubbles on single nanocatalysts in real time.[52] However, it is still a challenge to accurately localize the position of nanobubbles in real time. As a result, the local activity of nanocatalysts for gas-generating catalysis has yet been achieved by localizing the nanobubbles.

This research used the super-resolution microscopy to track single nanobubbles and reveal their local activity distribution around a Pd−Ag nanoplate (NP) (Figure 1a). The results show that the center of single nanobubbles can be localized to nanometer accuracy by the super-resolution microscopy. The relationship between the location, lifetime, and turnover rate of nanobubbles was also carefully studied.

In principle, the center of a single nanobubble can be precisely localized by using a 2D Gaussian function to fit its scattering image (Figure 1a). Because the scattering of the nanobubble occurs at the three-phase interface of gas, solution, and glass, the scattering center will be the geometric center of the nanobubble. The problem with localizing the scattering

Received: July 26, 2018
Accepted: September 6, 2018
Published: September 6, 2018

DOI: 10.1021/acs.jpclett.8b02302
J. Phys. Chem. Lett. 2018, 9, 5630−5635

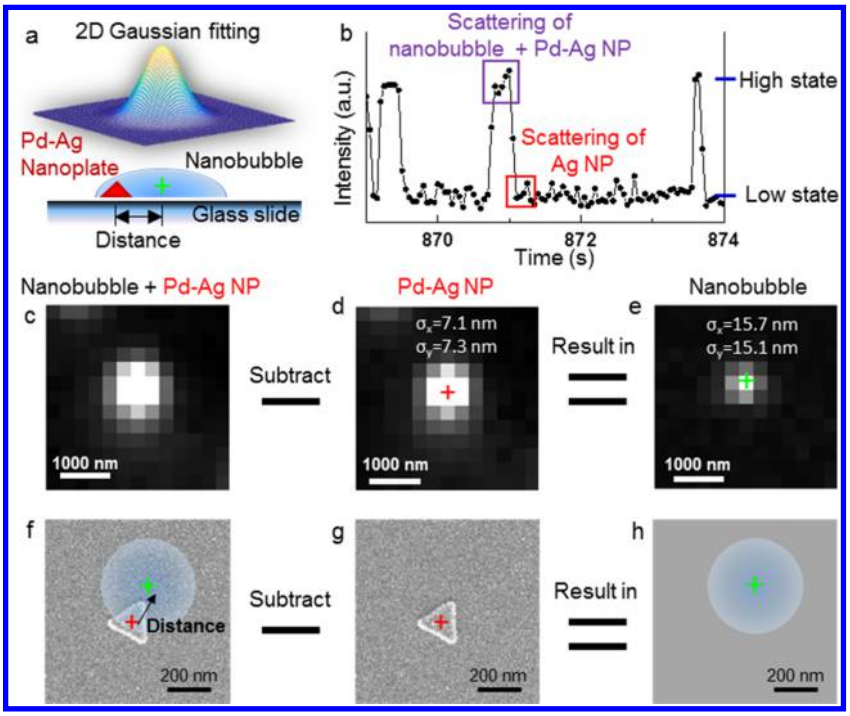

Figure 1. Tracking the center of a single nanobubble with the super-resolution microscopy. (a) Scheme of localizing the center of the single nanobubble by fitting its scattering signal with a 2D Gaussian function. (b) Scattering intensity trajectory of a single Pd−Ag nanoplate generating nanobubbles through the decomposition of 1.67 M HCOOH. (c) Dark-field microscopic image of a single Pd−Ag nanoplate with a nanobubble. The image is the combination of all frames in a high state, as shown in the purple square of panel b. (d) Dark-field image of a single Pd−Ag nanoplate. The image is the combination of the same number of frames in the following low state, as shown in the red square of panel b (or the calculation if the number of frames in the following low state is less than that in the high state; see Supporting Information SI.4 and SI.6 for the details.). The red cross is the center of the nanoplate, which is calculated by a 2D Gaussian fitting. The error bars for x and y directions are σ_x = 7.1 nm and σ_y = 7.3 nm, respectively. (e) Emission of the nanobubble by subtracting panel d from panel c. The green cross is the center of the nanobubble, which is calculated by a 2D Gaussian fitting. The error bars for x and y directions are σ_x = 15.7 nm and σ_y = 15.1 nm, respectively. (f) SEM image of the Pd−Ag nanoplate in panel c, overlapping a schematic nanobubble to illustrate the relation between the nanoplate and the nanobubble. (g) SEM image of the Pd−Ag nanoplate in panel d. (h) Schematic of a nanobubble.

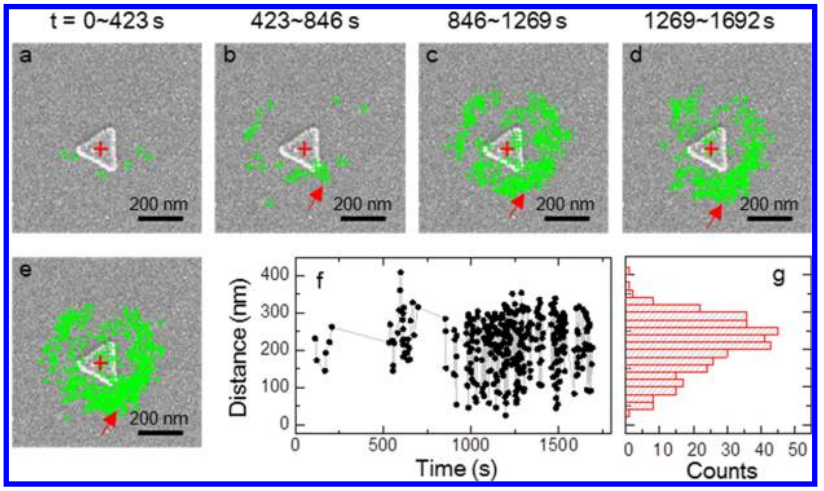

Figure 2. Distribution of nanobubble centers for a sample Pd−Ag nanoplate at different times. (a) From 0 to 423 s. Green and red crosses are for the centers of the nanobubbles and the Pd−Ag nanoplate, respectively. (b) From 423 to 846 s. (c) From 846 to 1269 s. (d) From 1269 to 1693 s. (e) Entire time from 0 to 1693 s. (f) Distance variation of the nanobubble centers at different times. (g) Histogram of the distance distribution.

center of the nanobubble with a 2D Gaussian function, however, is that the scattering signal of the nanobubble is always overlapped by the scattering of the Pd−Ag nanoplate, and so the scattering image of the nanobubble cannot be directly taken in the experiment. Therefore, a method is needed to obtain the scattering image of the nanobubble first before doing the fitting.

Figure 1b shows that the scattering intensity sharply increases when a nanobubble is generated on a single Pd−Ag nanoplate and then suddenly drops when the nanobubble dissolves. The scattering intensity variation also can be directly observed in the DFM images (Figure 1c,d). Figure 1c indicates that the scattering pattern of the combination of the nanobubble and the Pd−Ag nanoplate is a point spread

DOI: 10.1021/acs.jpclett.8b02302
J. Phys. Chem. Lett. 2018, 9, 5630−5635

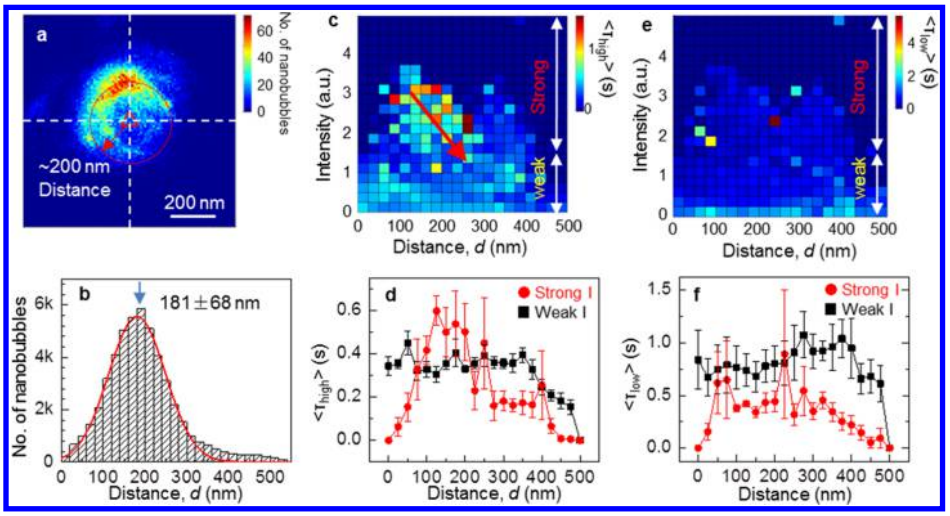

Figure 3. Super-resolution imaging of a large number of nanobubbles from many Pd−Ag nanoplates at the FA concentration of 1.67 M. (a) Relative location of the centers of the many nanobubbles to their Pd−Ag nanoplates. The plot includes about 52700 nanobubbles from 81 nanoplates. Pixel size is 10 nm × 10 nm. (b) Distance distribution of the centers of the nanobubbles to the Pd−Ag nanoplates. The red curve is the Gaussian fitting of the histogram. The error bar is the standard deviation. (c) Relationship between the distance, the scattering intensity of the nanobubbles, and the wait time of the high state ($<\tau_{high}>$). (d) Distribution of $<\tau_{high}>$ along the distance for the nanobubbles with strong and weak scattering intensity states. The threshold for the strong and weak scattering intensity states is 1.5, as shown in panel c. (e) Relationship between the distance, the scattering intensity of the nanobubbles, and the wait time of the low state ($<\tau_{low}>$). (f) Distribution of $<\tau_{low}>$ along the distance for the nanobubbles with strong and weak scattering intensity states. Next, the relationship of the distance, the scattering intensity of the nanobubbles, and the wait times ($<\tau_{high}>$ and $<\tau_{low}>$; the sign < > means average) was investigated. It should be mentioned that the intensity of a nanobubble is proportional to its size and that the physical meanings of τ_{high} and τ_{low} are the lifetime of the nanobubbles and the nucleation time of a nanobubble ($\tau_{nucleation}$), respectively.[52] Moreover, the nucleation rate of nanobubbles (J), which is proportional to the activity of nanocatalyst, is the reverse of the average nucleation time, that is, $<\tau_{nucleation}>^{-1}$, on a single Pd−Ag nanocatalyst.

function (PSF) because the sizes of both the nanobubble and the Pd−Ag nanoplate are less than the diffraction-limited resolution of an optical microscope. Therefore, it is hard to precisely and directly determine the location of the nanobubble from the information in Figure 1c.

To get the scattering image of just the nanobubble, we subtracted the scattering signal of the Pd−Ag nanoplate (as seen in Figure 1d) from the combined scattering signal of the Pd−Ag nanoplate and the nanobubble shown in Figure 1c. Figure 1e shows the resultant scattering signal of the nanobubble only. The result of separating the combined scattering images of both the Pd−Ag nanoplate and the nanobubble shown in Figure 1f can be seen as the separate images of the Pd−Ag nanoplate in Figure 1g and of the nanobubble in Figure 1h.

After separating the two scattering images, the images for both the Pd−Ag nanoplate (Figure 1d) and the nanobubble (Figure 1e) were fitted with a 2D Gaussian function (Supporting Information SI.4) to obtain their geometric centers, seperately. The centers of the fitting for both the Pd−Ag nanoplate (marked with a red cross in Figure 1d,g) and the nanobubble (marked with a green cross in Figure 1e,h) are their geometric centers. By means of the aforementioned treatment and calculation, the relative location of the nanobubble to the Pd−Ag nanoplate can clearly be identified, as shown in Figure 1f. Using the fitting, the precision of the localization for both the nanoplate and the nanobubble can be from several to tens of nanometers depending on the intensity of their scattering (Figure 1d,e). For example, the error bars of the center of the Pd−Ag nanoplate for x and y directions are σ_x = 7.1 nm and σ_y = 7.3 nm, respectively, whereas the error bars of the center of the nanobubble are σ_x = 15.7 nm and σ_y = 15.1 nm, respectively. If the treatment above is applied to all of the nanobubbles appearing in Figure 1b, the locations for them all can be determined by this super-resolution microscopy. To get a more detailed picture of the appearance of the nanobubbles, their center distribution was plotted for a sample Pd−Ag nanoplate at different times (Figure 2a−d). The number of nanobubbles varies at different periods (Figure 2a−d) due to the catalytic activity variation of the single Pd−Ag nanoplate. Figure 2e also shows the center distribution of the nanobubbles for the entire period from 0 to 1693 s. It can be seen from Figure 2a−e that the centers of the nanobubbles do not appear exactly on top of the Pd−Ag nanoplate; instead, they spread out in a large range around it.

According to our previous study,[52] the rate of nanobubbles generation is related to higher gas concentration around the single Pd−Ag catalyst. Usually, the higher gas concentration is induced by higher local activity of nanocatalyst. Therefore, we can at least qualitatively correlate the location of the nanobubble generation with the position of the active sites of the catalyst. Also notable is that the bottom right tip of the Pd−Ag nanoplate (indicated by the red arrow) shows many more nanobubble centers, indicating higher activity on that tip. Other examples in Figure S4 also show similar results. This is consistent with previous research findings that the tips of nanocatalysts usually have higher activity due to having more defects.[53]

Figure 2f shows that the distances between the centers of the nanobubbles and the center of the nanoplate vary with time. Nevertheless, they are always in a certain range from 0 to ∼400 nm, which can be directly monitored, as seen in Figure 2e. Figure 2g shows the histogram of the distance distribution, which exhibits a maximum population at ∼200 nm. Because the nanobubble covers both the nanoplate and the center of the bubble, the radius of the nanobubble is larger than the

DOI: 10.1021/acs.jpclett.8b02302
J. Phys. Chem. Lett. 2018, 9, 5630−5635

distance. Therefore, the radius for most nanobubbles is at least 200 nm, and the size of the nanobubbles can be >400 nm. Nevertheless, the thickness of the nanobubbles is usually very thin because their contact angle is much lower than the expected contact angle in Young's law.[54,55] So the bubbles still can be regarded as nanobubbles.

The distribution of the nanobubbles around the nanoplates can be determined by setting the centers of the nanoplates as the base point and then plotting the centers of a number of nanobubbles from the different plates, as shown in Figure 3a. It should be mentioned that all of the nanoplates share the same center, and the plot will clearly exhibit the distance between the center position of the nanobubble and the center position of the catalyst. Therefore, the different (sharp angle, shape, and size) nanoplates have no influence on this distance during our overlapping. The center position of nanoplates in Figure 3a is at the crossing of the two white lines. Similar to the result in Figure 2e, the distances between the nanobubble centers and the nanoplate mainly distribute near 200 nm (Figure 3a).

However, the overall distributions of the bubbles phase are not three-fold symmetric, even though the catalyst is mostly triangular. This is due to the fact that the orientation of nanoplates is randomly distributed when immobilizing the nanoplate catalyst on the glass slide by dropping the diluted nanoplate solution on slide. Hence, even if the catalysts have higher activity near the tip, the distribution of activity will be random around the original point of overlapping. On another aspect, Figure 2 also shows that the activity distributes not only near the tips but also on other locations of nanoplate. Because of this reason, we may not get three-fold symmetry after the overlapping in Figure 3a.

To get the precise distance, a histogram of the distance distribution of the centers of the nanobubbles to the Pd−Ag nanoplates is plotted in Figure 3b. The maximum distribution is found with a Gaussian fitting to be 181 ± 68 nm. This is a very interesting phenomenon because it indicates that the nanobubble tends to be generated at a certain distance from the catalyst but not on top of the catalyst. The distance causes the nanobubble to not totally cover the catalyst, which facilitates the mass transfer of the reactant. The distance also presents a way to point out the active sites for the catalytic reaction.

First, Figure 3c shows the relationship between the distance, the scattering intensity of the nanobubbles, and the wait time of the high state ($<\tau_{high}>$). In Figure 3c, the distance between the nanobubbles and the Pd−Ag nanoplate does not show any obvious correlation with the intensity of the nanobubbles. This indicates that nanobubbles of different sizes could randomly appear at any distance around the Pd−Ag nanoplate.

Additionally, Figure 3d shows the division of the nanobubbles into two populations according to the scattering intensity, that is, the size of the nanobubbles.[52] The threshold for strong and weak intensities is set at 1.5. For low-intensity (small size, <1.5) nanobubbles, the $<\tau_{high}>$ almost keeps a constant value within 350 nm but decreases from 350 to 500 nm. This means that small nanobubbles have similar lifetime lengths when appearing at a distance of 350 nm or less, but the lifetimes sharply decrease when the distance is farther than 350 nm. The nanobubble is in a state of dynamic equilibrium. When the distance is too large, the nanobubble has less contact with the nanoplate, and it will harvest less product gas from it. When there is too little gas to support the nanobubble, it will dissolve.

For high-intensity (i.e., large size) nanobubbles in Figure 3d, the $<\tau_{high}>$ shows a volcano behavior with the distance and has a peak at ∼150 nm, which is higher than that of small nanobubbles. This indicates that the nanobubbles appearing at such distances have longer lifetimes, that is, higher stability. When the scattering intensity, or size, of a nanobubble has a fixed large size, either too large or too small a distance will cause shorter lifetimes. If the distance is too large, then the nanobubble will have less contact with the nanoplate, and it will harvest less product gas from it. On the contrary, if the distance is too small, then the nanobubble will have too much contact with the nanoplate and may even cover the total plate. When a nanobubble covers the entire nanoplate, it will block the reactant solution and impedes the mass transfer of the reactant (Figure 3d). Therefore, it is easy to see that the lifetime of the nanobubble, that is, $<\tau_{high}>$, will be shorter with this scenario.

Second, Figure 3e shows the relation of the distance, intensity, and $<\tau_{low}>$ of the nanobubbles. The nanobubbles can also be divided into two populations according to the scattering intensity of 1.5, as shown in Figure 3f. For low-intensity (small size, <1.5) nanobubbles, the $<\tau_{low}>$ keeps an almost constant value within 350 nm and decreases from 350 to 500 nm (Figure 3f). This means that small nanobubbles from catalysts of either high or low activity can randomly appear within 350 nm, but only the highly active catalysts can cause small nanobubbles to appear farther than 350 nm. Long distance may be due to more energy being released from the catalytic reaction, which could blow the nanobubble far away.

The $<\tau_{low}>$ for high-intensity (large size) nanobubbles also shows a volcano behavior with the distance and has a high stage from about 50 to 250 nm, a value similar to that of small nanobubbles (Figure 3f). This indicates that both large and small nanobubbles appearing at such distances show similar activity. Moreover, the $<\tau_{low}>$ of large nanobubbles decreases sharply after 300 nm, which is also similar to small nanobubbles, indicating that large nanobubbles from highly active catalysts could appear farther than 300 nm. Figure 3f also shows that large nanobubbles from highly active catalysts also tend to appear on top of the catalyst.

This research used 2D Gaussian fitting to localize the center of individual nanobubbles and reveal the local activity distribution with from several to tens of nanometers accuracy. Also, it was found that the distances between the centers of the nanobubbles and the center of the nanoplate usually distribute in a certain range from 0 to 500 nm and vary with time. The histogram of this distance distribution exhibits a maximum population at ∼200 nm. In addition, the tips of the Pd−Ag nanoplate were found to be more active than the edges. The research further reveals that small nanobubbles usually behave differently from large ones. Unlike large nanobubbles, small ones usually show stable lifetime and turnover rates within a certain distance but show shorter lifetime and higher turnover rates when farther than that distance. Large nanobubbles usually show a volcano behavior with the distance. This work presents an effective, high-resolution method for localizing the position of nanocatalysts.

■ ASSOCIATED CONTENT

Supporting Information

The Supporting Information is available free of charge on the ACS Publications website at DOI: 10.1021/acs.jpclett.8b02302.

DOI: 10.1021/acs.jpclett.8b02302
J. Phys. Chem. Lett. 2018, 9, 5630−5635

Details of materials and characterizatons, synthesis of Pd−Ag nanoplate catalyst, dark-field imaging of single Pd−Ag nanoplate catalysis, locating the center of single nanobubble with super-resolution microscopy, discussion of the size and relative location of nanobubbles, dark-field image of a single Pd−Ag nanoplate (Figure S1), distribution of the centers of nanobubble along the angle to Pd−Ag nanoplates (Figure S2), trajectory for example Pd−Ag nanoplates (Figure S3), more examples for the locations of nanobubbles and Pd−Ag nanoplates (Figure S4), and parameters for fitting (Table S1) (PDF)

AUTHOR INFORMATION

Corresponding Authors

*E-mail: xczhou2013@sinano.ac.cn (X.Z.).
*E-mail: yjhuang@cug.edu.cn (Y.H.).

ORCID

Xiaochun Zhou: 0000-0001-9793-6072

Notes

The authors declare no competing financial interest.

ACKNOWLEDGMENTS

We are grateful for financial support granted by the Ministry of Science and Technology of China (nos. 2016YFE0105700, 2016YFA0200700), the National Natural Science Foundation of China (nos. 21373264, 21573275), the Natural Science Foundation of Jiangsu Province (BK20150362), Suzhou Institute of Nanotech and Nanobionics (Y3AAA11004), China Postdoctoral Science Foundation (no. 2018M632406), Thousand Youth Talents Plan (Y3BQA11001), and the Fundamental Research Funds for the Central Universities (China University of Geosciences (Wuhan), CUG140610 and CUG170102). This work was sponsored by the Collaborative Innovation Center of Suzhou Nano Science and Technology.

REFERENCES

(1) Zhang, Q.; Wang, H. Facet-Dependent Catalytic Activities of Au Nanoparticles Enclosed by High-Index Facets. *ACS Catal.* **2014**, *4*, 4027−4033.

(2) Zhou, X.; Andoy, N. M.; Liu, G.; Choudhary, E.; Han, K. S.; Shen, H.; Chen, P. Quantitative Super-Resolution Imaging Uncovers Reactivity Patterns on Single Nanocatalysts. *Nat. Nanotechnol.* **2012**, *7*, 237−241.

(3) Blythe, K. L.; Titus, E. J.; Willets, K. A. Triplet-State-Mediated Super-Resolution Imaging of Fluorophore-Labeled Gold Nanorods. *ChemPhysChem* **2014**, *15*, 784−793.

(4) Tachikawa, T.; Yamashita, S.; Majima, T. Evidence for Crystal-Face-Dependent TiO_2 Photocatalysis from Single-Molecule Imaging and Kinetic Analysis. *J. Am. Chem. Soc.* **2011**, *133*, 7197−7204.

(5) Sun, Y.; Yin, Y.; Mayers, B. T.; Herricks, T.; Xia, Y. Uniform Silver Nanowires Synthesis by Reducing $AgNO_3$ with Ethylene Glycol in the Presence of Seeds and Poly(Vinyl Pyrrolidone). *Chem. Mater.* **2002**, *14*, 4736−4745.

(6) Duan, H.; Wang, D.; Li, Y. Green Chemistry for Nanoparticle Synthesis. *Chem. Soc. Rev.* **2015**, *44*, 5778−5792.

(7) Hu, Y.; Wu, P.; Yin, Y.; Zhang, H.; Cai, C. Effects of Structure, Composition, and Carbon Support Properties on the Electrocatalytic Activity of Pt-Ni-Graphene Nanocatalysts for the Methanol Oxidation. *Appl. Catal., B* **2012**, *111*, 208−217.

(8) Fu, X. Z.; Liang, Y.; Chen, S. P.; Lin, J. D.; Liao, D. W. Pt-Rich Shell Coated Ni Nanoparticles as Catalysts for Methanol Electro-Oxidation in Alkaline Media. *Catal. Commun.* **2009**, *10*, 1893−1897.

(9) Zhou, Y.; Zhu, Y.; Wang, Z. Q.; Zou, S.; Ma, G.; Xia, M.; Kong, X.; Xiao, L.; Gong, X. Q.; Fan, J. Catalytic Activity Control Via Crossover between Two Different Microstructures. *J. Am. Chem. Soc.* **2017**, *139*, 13740−13748.

(10) Komeda, T.; Manassen, Y. Distribution of Frequencies of a Single Precessing Spin Detected by Scanning Tunneling Microscope. *Appl. Phys. Lett.* **2008**, *92*, 212506.

(11) Donnet, J. B.; Papirer, E.; Wang, W.; Stoeckli, H. F. The Observation of Active Carbons by Scanning Tunneling Microscopy. *Carbon* **1994**, *32*, 183−184.

(12) Rust, M. J.; Bates, M.; Zhuang, X. Sub-Diffraction-Limit Imaging by Stochastic Optical Reconstruction Microscopy (STORM). *Nat. Methods* **2006**, *3*, 793−795.

(13) Chen, X.; Maljusch, A.; Rincon, R. A.; Battistel, A.; Bandarenka, A. S.; Schuhmann, W. Local Visualization of Catalytic Activity at Gas Evolving Electrodes Using Frequency-Dependent Scanning Electrochemical Microscopy. *Chem. Commun. (Cambridge, U. K.)* **2014**, *50*, 13250−13253.

(14) Zhou, X.; Andoy, N. M.; Liu, G.; Choudhary, E.; Han, K. S.; Shen, H.; Chen, P. Quantitative Super-Resolution Imaging Uncovers Reactivity Patterns on Single Nanocatalysts. *Nat. Nanotechnol.* **2012**, *7*, 237−241.

(15) Zhang, Y. W.; Lucas, J. M.; Song, P.; Beberwyck, B.; Fu, Q.; Xu, W. L.; Alivisatos, A. P. Superresolution Fluorescence Mapping of Single-Nanoparticle Catalysts Reveals Spatiotemporal Variations in Surface Reactivity. *Proc. Natl. Acad. Sci. U. S. A.* **2015**, *112*, 8959−8964.

(16) Borkent, B. M.; Dammer, S. M.; Schonherr, H.; Vancso, G. J.; Lohse, D. Superstability of Surface Nanobubbles. *Phys. Rev. Lett.* **2007**, *98*, 204502.

(17) Hohlbein, J.; Gryte, K.; Heilemann, M.; Kapanidis, A. N. Surfing on a New Wave of Single-Molecule Fluorescence Methods. *Phys. Biol.* **2010**, *7*, 031001.

(18) Zhang, Z.; Kenny, S. J.; Hauser, M.; Li, W.; Xu, K. Ultrahigh-Throughput Single-Molecule Spectroscopy and Spectrally Resolved Super-Resolution Microscopy. *Nat. Methods* **2015**, *12*, 935−938.

(19) Feinergracia, N.; Beck, M.; Pujals, S.; Tosi, S.; Mandal, T.; Buske, C.; Linden, M.; Albertazzi, L. Super-Resolution Microscopy Unveils Dynamic Heterogeneities in Nanoparticle Protein Corona. *Small* **2017**, *13*, 1701631.

(20) Taylor, A.; Verhoef, R.; Beuwer, M.; Wang, Y.; Zijlstra, P. All-Optical Imaging of Gold Nanoparticle Geometry Using Super-Resolution Microscopy. *J. Phys. Chem. C* **2018**, *122*, 2336−2342.

(21) Stranahan, S. M.; Willets, K. A. Super-Resolution Optical Imaging of Single-Molecule SERS Hot Spots. *Nano Lett.* **2010**, *10*, 3777−3784.

(22) Weber, M. L.; Willets, K. A. Correlated Super-Resolution Optical and Structural Studies of Surface-Enhanced Raman Scattering Hot Spots in Silver Colloid Aggregates. *J. Phys. Chem. Lett.* **2011**, *2*, 1766−1770.

(23) Willets, K. A. Super-Resolution Imaging of SERS Hot Spots. *Chem. Soc. Rev.* **2014**, *43*, 3854−3864.

(24) Wu, Y.; Yuan, B.; Li, M.; Zhang, W. H.; Liu, Y.; Li, C. Well-Defined Biocl Colloidal Ultrathin Nanosheets: Synthesis, Characterization, and Application in Photocatalytic Aerobic Oxidation of Secondary Amines. *Chem. Sci.* **2015**, *6*, 1873−1878.

(25) Walter, M. G.; Warren, E. L.; McKone, J. R.; Boettcher, S. W.; Mi, Q.; Santori, E. A.; Lewis, N. S. Solar Water Splitting Cells. *Chem. Rev.* **2010**, *110*, 6446−6473.

(26) Yang, X. Y.; Wolcott, A.; Wang, G. M.; Sobo, A.; Fitzmorris, R. C.; Qian, F.; Zhang, J. Z.; Li, Y. Nitrogen-Doped ZnO Nanowire Arrays for Photoelectrochemical Water Splitting. *Nano Lett.* **2009**, *9*, 2331−2336.

(27) Fang, Y.; Li, Z.; Jiang, Y.; Wang, X.; Chen, H. Y.; Tao, N.; Wang, W. Intermittent Photocatalytic Activity of Single CdS Nanoparticles. *Proc. Natl. Acad. Sci. U. S. A.* **2017**, *114*, 10566−10571.

(28) Carmo, M.; Fritz, D. L.; Mergel, J.; Stolten, D. A Comprehensive Review on PEM Water Electrolysis. *Int. J. Hydrogen Energy* **2013**, *38*, 4901−4934.

DOI: 10.1021/acs.jpclett.8b02302
J. Phys. Chem. Lett. 2018, 9, 5630−5635

(29) Celaje, J. J. A.; Lu, Z. Y.; Kedzie, E. A.; Terrile, N. J.; Lo, J. N.; Williams, T. J. A Prolific Catalyst for Dehydrogenation of Neat Formic Acid. *Nat. Commun.* **2016**, *7*, 11308−11308.
(30) Jiang, K.; Xu, K.; Zou, S.; Cai, W. B. B-Doped Pd Catalyst: Boosting Room-Temperature Hydrogen Production from Formic Acid-Formate Solutions. *J. Am. Chem. Soc.* **2014**, *136*, 4861−4864.
(31) Mori, K.; Tanaka, H.; Dojo, M.; Yoshizawa, K.; Yamashita, H. Synergic Catalysis of PdCu Alloy Nanoparticles within a Macroreticular Basic Resin for Hydrogen Production from Formic Acid. *Chem. - Eur. J.* **2015**, *21*, 12085−12092.
(32) Singh, A. K.; Jang, S.; Kim, J. Y.; Sharma, S.; Basavaraju, K. C.; Kim, M. G.; Kim, K. R.; Lee, J. S.; Lee, H. H.; Kim, D. P. One-Pot Defunctionalization of Lignin-Derived Compounds by Dual-Functional Pd50Ag50/Fe_3O_4/N-rGO Catalyst. *ACS Catal.* **2015**, *5*, 6964−6972.
(33) Yan, J. M.; Wang, Z. L.; Gu, L.; Li, S. J.; Wang, H. L.; Zheng, W. T.; Jiang, Q. AuPd-MnOx/MOF-Graphene: An Efficient Catalyst for Hydrogen Production from Formic Acid at Room Temperature. *Adv. Energy Mater.* **2015**, *5*, 1500107−1500107.
(34) Yu, W. Y.; Mullen, G. M.; Flaherty, D. W.; Mullins, C. B. Selective Hydrogen Production from Formic Acid Decomposition on Pd-Au Bimetallic Surfaces. *J. Am. Chem. Soc.* **2014**, *136*, 11070−11078.
(35) Zhou, X.; Huang, Y.; Xing, W.; Liu, C.; Liao, J.; Lu, T. High-Quality Hydrogen from the Catalyzed Decomposition of Formic Acid by Pd-Au/C and Pd-Ag/C. *Chem. Commun.* **2008**, 3540−3542.
(36) Wasmus, S.; Kuver, A. Methanol Oxidation and Direct Methanol Fuel Cells: A Selective Review. *J. Electroanal. Chem.* **1999**, *461*, 14−31.
(37) Badwal, S. P. S.; Giddey, S.; Kulkarni, A.; Goel, J.; Basu, S. Direct Ethanol Fuel Cells for Transport and Stationary Applications - A Comprehensive Review. *Appl. Energy* **2015**, *145*, 80−103.
(38) Yu, X.; Pickup, P. G. Recent Advances in Direct Formic Acid Fuel Cells (DFAFC). *J. Power Sources* **2008**, *182*, 124−132.
(39) Hao, R.; Fan, Y.; Howard, M. D.; Vaughan, J. C.; Zhang, B. Imaging Nanobubble Nucleation and Hydrogen Spillover During Electrocatalytic Water Splitting. *Proc. Natl. Acad. Sci. U. S. A.* **2018**, *115*, 5878−5883.
(40) Su, H.; Fang, Y.; Chen, F.; Wang, W. Monitoring the Dynamic Photocatalytic Activity of Single CdS Nanoparticles by Lighting up H_2 Nanobubbles with Fluorescent Dyes. *Chem. Sci.* **2018**, *9*, 1448−1453.
(41) Wang, W. Imaging the Chemical Activity of Single Nanoparticles with Optical Microscopy. *Chem. Soc. Rev.* **2018**, *47*, 2485−2508.
(42) Chen, Q.; Wiedenroth, H. S.; German, S. R.; White, H. S. Electrochemical Nucleation of Stable N_2 Nanobubbles at Pt Nanoelectrodes. *J. Am. Chem. Soc.* **2015**, *137*, 12064−12069.
(43) Luo, L.; White, H. S. Electrogeneration of Single Nanobubbles at Sub-50-nm-radius Platinum Nanodisk Electrodes. *Langmuir* **2013**, *29*, 11169−11175.
(44) Li, D.; Pan, Y.; Zhao, X.; Bhushan, B. Study on Nanobubble-On-Pancake Objects Forming at Polystyrene/Water Interface. *Langmuir* **2016**, *32*, 11256−11264.
(45) Lou, S. T.; Ouyang, Z. Q.; Zhang, Y.; Li, X. J.; Hu, J.; Li, M. Q.; Yang, F. J. Nanobubbles on Solid Surface Imaged by Atomic Force Microscopy. *J. Vac. Sci. Technol., B: Microelectron. Process. Phenom.* **2000**, *18*, 2573−2575.
(46) Tyrrell, J. W. G.; Attard, P. Images of Nanobubbles on Hydrophobic Surfaces and Their Interactions. *Phys. Rev. Lett.* **2001**, *87*, 176140.
(47) Ishida, N.; Inoue, T.; Miyahara, M.; Higashitani, K. Nano Bubbles on a Hydrophobic Surface in Water Observed by Tapping-Mode Atomic Force Microscopy. *Langmuir* **2000**, *16*, 6377−6380.
(48) Chen, Q.; Luo, L.; Faraji, H.; Feldberg, S. W.; White, H. S. Electrochemical Measurements of Single H_2 Nanobubble Nucleation and Stability at Pt Nanoelectrodes. *J. Phys. Chem. Lett.* **2014**, *5*, 3539−3544.
(49) Chan, C. U.; Ohl, C. D. Total-Internal-Reflection-Fluorescence Microscopy for the Study of Nanobubble Dynamics. *Phys. Rev. Lett.* **2012**, *109*, 174501−174501.
(50) Zhang, X. H.; Khan, A.; Ducker, W. A. A Nanoscale Gas State. *Phys. Rev. Lett.* **2007**, *98*, 136101−136101.
(51) Fang, Z.; Zhen, Y. R.; Neumann, O.; Polman, A.; García de Abajo, F. J.; Nordlander, P.; Halas, N. J. Evolution of Light-Induced Vapor Generation at a Liquid-Immersed Metallic Nanoparticle. *Nano Lett.* **2013**, *13*, 1736−1742.
(52) Li, S.; Du, Y.; He, T.; Shen, Y.; Bai, C.; Ning, F.; Hu, X.; Wang, W.; Xi, S.; Zhou, X. Nanobubbles: An Effective Way to Study Gas-Generating Catalysis on a Single Nanoparticle. *J. Am. Chem. Soc.* **2017**, *139*, 14277−14284.
(53) Du, Y.; He, X.; Zhan, Y.; Li, S.; Shen, Y.; Ning, F.; Yan, L.; Zhou, X. Imaging the Site-Specific Activity and Kinetics on a Single Nanomaterial by Microchamber Array. *ACS Catal.* **2017**, *7*, 3607−3614.
(54) Borkent, B. M.; de Beer, S.; Mugele, F.; Lohse, D. On the Shape of Surface Nanobubbles. *Langmuir* **2010**, *26*, 260−268.
(55) Zhang, X. H.; Maeda, N.; Craig, V. S. J. Physical Properties of Nanobubbles on Hydrophobic Surfaces in Water and Aqueous Solutions. *Langmuir* **2006**, *22*, 5025−5035.

DOI: 10.1021/acs.jpclett.8b02302
J. Phys. Chem. Lett. 2018, 9, 5630−5635